

DESY 97-248
December 1997

ISSN 0418-9833

THE STRUCTURE OF HADRONS

Vladimir CHEKELIAN (SHEKELYAN)

ITEP (Moscow)

E-mail: shekeln@mail.desy.de

Abstract

Recent experimental results contributing to the understanding of the structure of the nucleon are reviewed. They include the final NMC ($\mu N \rightarrow \mu X$) results on proton and deuteron structure functions ; a re-analysis of the CCFR ($\nu\text{Fe} \rightarrow lX$) data on F_2 and xF_3 ; new preliminary results from CDF on charge asymmetry in W production, from E866 on Drell-Yan μ -pair production and from E706 on prompt photon production. New results from HERA on F_2 , on the gluon density at low x , on the charm contribution $F_2^{c\bar{c}}$, on a determination of F_L and on measurements in the very low Q^2 region are discussed.

*Invited talk at the 18th International Symposium on Lepton-Photon Interactions,
Hamburg, July 1997*

arXiv:hep-ph/9712539v1 29 Dec 1997

THE STRUCTURE OF HADRONS

Vladimir CHEKELIAN (SHEKELYAN)

ITEP (Moscow)

E-mail: shekeln@mail.desy.de

Recent experimental results contributing to the understanding of the structure of the nucleon are reviewed. They include the final NMC ($\mu N \rightarrow \mu X$) results on proton and deuteron structure functions ; a re-analysis of the CCFR ($\nu\text{Fe} \rightarrow lX$) data on F_2 and xF_3 ; new preliminary results from CDF on charge asymmetry in W production, from E866 on Drell-Yan μ -pair production and from E706 on prompt photon production. New results from HERA on F_2 , on the gluon density at low x , on the charm contribution $F_2^{c\bar{c}}$, on a determination of F_L and on measurements in the very low Q^2 region are discussed.

1 Introduction

The study of the structure of hadrons has been always of great importance for the development of high energy physics. This report concentrates on recent experimental contributions to the understanding of the nucleon structure ^a. Two main questions have been addressed in such studies. Firstly, a test of the theory of strong interactions and, secondly, a determination of the momentum distributions of the partons within the nucleon.

The main sources of experimental information on the structure of the nucleon are the fixed target experiments with electron, muon, neutrino and proton beams, the $p\bar{p}$ colliders and the ep collider at HERA.

Since the initial observation ¹ of Bjorken scaling, experiments on Deep Inelastic Scattering (DIS) play an outstanding role in the investigation of the nucleon structure. This observation established that the quark-parton model is a valid framework for the interpretation of data and that the DIS structure functions from different processes can be expressed in terms of universal parton densities. The later observation of scaling violation ² and identification of partons as quarks and gluons has confirmed the field theory of quarks and gluons and their strong interactions, Quantum Chromodynamics (QCD). QCD in conjunction with electroweak theory constitutes now the Standard Model of elementary particle physics.

The differential cross section for neutral current deep inelastic scattering of a charged lepton on a nucleon is related to the three structure functions F_2 , F_L and xF_3 according to

$$\frac{d^2\sigma^{l\pm N}}{dx dQ^2} = \frac{2\pi\alpha^2}{Q^4 x} [(1 + (1 - y)^2)F_2(x, Q^2) - y^2 F_L(x, Q^2) \mp (1 - (1 - y)^2)xF_3(x, Q^2)] \quad (1)$$

Here Q^2 is the squared four-momentum transfer between the lepton l and the nucleon N , x denotes the Bjorken variable, and $y = Q^2/xs$ is the inelasticity, where s is the center of mass energy squared of the collision and α is the fine structure constant. In eq. 1 it is assumed that s is much larger than the nucleon mass. For Q^2 much below the Z^0 mass squared, the parity violating structure function xF_3 is negligible and the structure function F_2 is given purely by photon exchange. The structure functions F_2 and F_L are related by $R = \sigma_L/\sigma_T \simeq F_L/(F_2 - F_L)$, where R is the ratio of cross sections of longitudinally and transversely polarized virtual photons. The contribution of the longitudinal structure function F_L to the cross section is important only at large y , typically $y \geq 0.4$. In the quark-parton model $F_L=0$, and F_2 is a sum over the quark and antiquark momentum fractions within a nucleon multiplied by the corresponding quark charge squared.

^aThe spin structure of the nucleon, diffraction and hadronic jet production are discussed at this conference in the talks given by A. Bruell, E. Gallo and H. Schellman. Theoretical aspects are reviewed by S. Catani.

In perturbative QCD the structure function F_2 is a convolution of the parton distributions and coefficient functions $C(x, Q^2)$

$$\frac{1}{x} F_2(x, Q^2) = \sum_{i=1}^{n_f} e_i^2 C_i(x, Q^2) \otimes (q_i(x, Q^2) + \bar{q}_i(x, Q^2)) + C_g(x, Q^2) \otimes g(x, Q^2), \quad (2)$$

where q_i denotes quarks of charge e_i and g gluons, \otimes stands for a convolution integral and n_f is the number of contributing flavors. The parton distributions evolve with Q^2 following the DGLAP³ equations

$$\frac{\partial}{\partial \ln Q^2} \begin{pmatrix} q \\ g \end{pmatrix} = \frac{\alpha_s(Q^2)}{2\pi} \begin{bmatrix} P_{qq} & P_{qg} \\ P_{gq} & P_{gg} \end{bmatrix} \otimes \begin{pmatrix} q \\ g \end{pmatrix}, \quad (3)$$

where α_s denotes the strong coupling constant. The coefficient functions C_i and splitting functions P_{ij} are obtained by perturbative expansion in a specific factorization and renormalization scheme.

The solution of the DGLAP evolution equation to next-to-leading order (NLO) together with the input parton distributions, which cannot be derived from first principles and should be fitted to data at some starting scale Q_0^2 , constitute the usual framework of a QCD analysis of the experimental results.

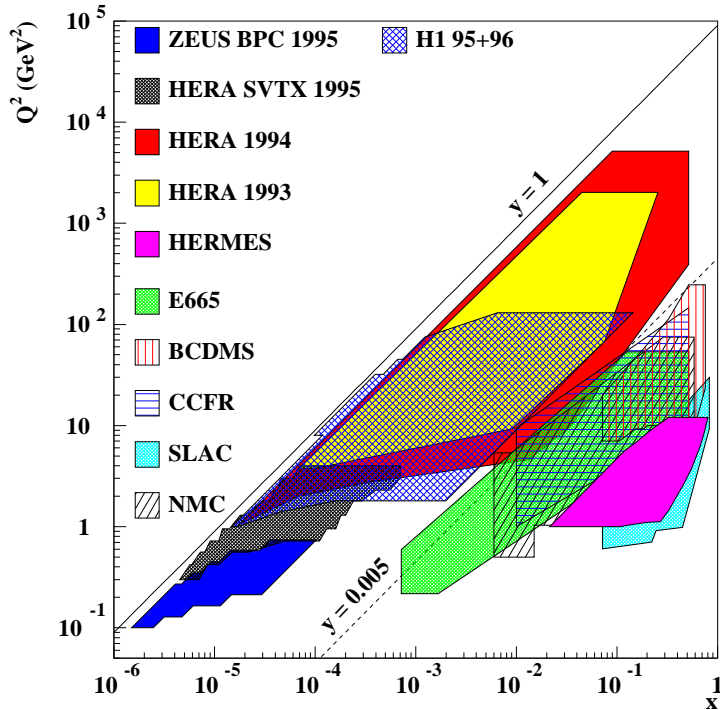


Figure 1: The regions in x and Q^2 covered by different DIS experiments.

The kinematic phase space covered by DIS experiments is summarized in Figure 1. The data span 6 orders of magnitude in x and 5 orders of magnitude in Q^2 and allow to make very precise tests of QCD, extract quark and gluon densities and determine α_s . Combined QCD analyses of the existing DIS information together with information from hadron-hadron collisions is a goal of NLO DGLAP fits such as performed by MRS^{4,5,6,7}, CTEQ^{8,9,10} and GRV¹¹.

The paper is organized as follows. In section 2, devoted to results from fixed target DIS experiments, the final NMC (μN) results and a re-analysis of the CCFR (νFe) data are presented.

Additional constraints on parton densities from hadron-hadron collisions are presented in section 3. Recent HERA results on F_2 , on the gluon density, on the charm contribution $F_2^{c\bar{c}}$ to the structure function of the proton, on the determination of F_L by H1 and on measurements in the very low Q^2 region are discussed in section 4, followed by a summary in section 5.

2 DIS in Fixed Target Experiments

Until a few years ago our knowledge of structure functions and derived quantities such as parton distributions was almost entirely based on the fixed target experiments, using electron, muon and neutrino beams.

2.1 The Final NMC Results ($\mu N \rightarrow \mu X$)

The New Muon Collaboration (NMC) at CERN has published final results^{12,13,14,15} on deep inelastic muon nucleon scattering at muon beam energies of 90, 120, 200, and 280 GeV.

The final NMC F_2^p and F_2^d data¹² for proton and deuteron targets (the results for F_2^d are shown in Figure 2) cover the kinematic range $0.002 < x < 0.6$ and $0.5 < Q^2 < 75 \text{ GeV}^2$ with high statistical accuracy and with systematic uncertainties between 1% and 5%. The coverage in x and Q^2 was extended to lower values due to the use of a small angle trigger. The results compare well with previous measurements from SLAC, BCDMS (see Figure 2) and E665 and extrapolate smoothly to the recent HERA data. The ratio R of cross sections of longitudinally and transversely polarized

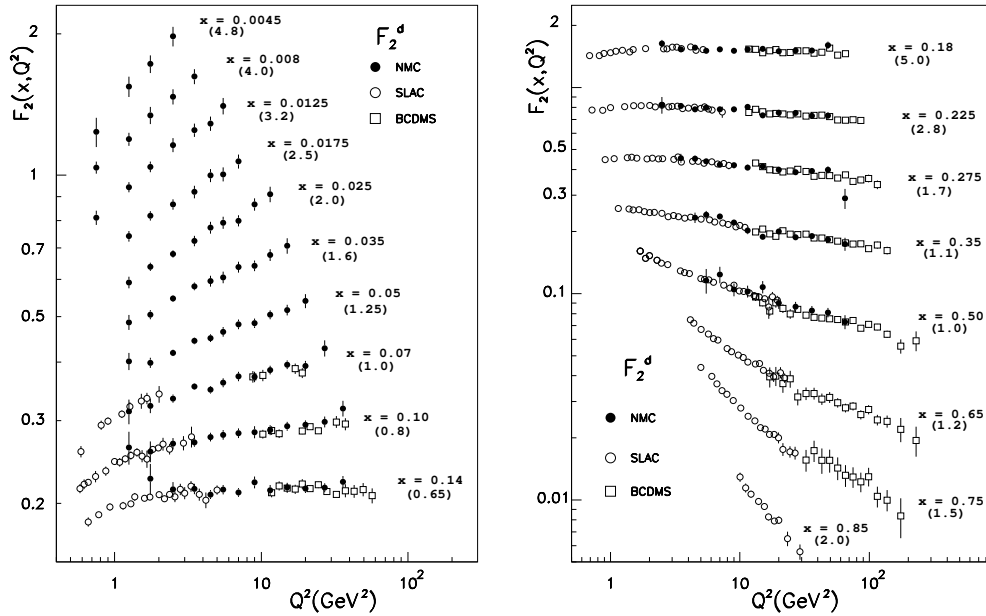


Figure 2: The final NMC results for F_2^d compared to SLAC and BCDMS results.

virtual photons was measured for $0.002 < x < 0.12$ and $1 < Q^2 < 25 \text{ GeV}^2$. The results are in agreement with earlier measurements as well as with expectations from perturbative QCD. The difference $(R^d - R^p)$ ¹³, determined for $0.003 < x < 0.35$, is compatible with zero as expected. The results for the structure function ratio F_2^d/F_2^p ¹³ cover the x range from 0.001 to 0.8 and the Q^2 range from 0.1 to 145 GeV^2 with a typical systematic accuracy of 0.5%. The data on F_2^d/F_2^p and

the F_2 parameterization¹⁶ have been used to determine the Gottfried sum $S_G = \int_0^1 (F_2^p - F_2^n) dx/x$. The result in the interval $0.004 < x < 0.8$ at $Q^2 = 4 \text{ GeV}^2$ is 0.2281 ± 0.0065 in agreement with the previous estimation¹⁷. The value obtained is below the expectation of $1/3$, indicating a flavor asymmetry in the quark-antiquark sea.

Nuclear effects were investigated studying the dependence on the mass number A in the shadowing region (small x), the enhancement region (at x about 0.1) and the EMC effect region (large x) by measuring with a series of different nuclei. A clear increase with A was observed for all effects¹⁴. A study of the Q^2 dependence of nuclear effects was performed using high luminosity measurements with thick carbon and tin targets¹⁵.

2.2 Re-analysis of the CCFR Data ($\nu\text{Fe} \rightarrow lX$)

Accurate νFe structure function data have been available for some time from the high statistics CCFR experiment at FNAL. In the earlier analysis¹⁸, the muon and hadron energy calibrations were determined using a Monte Carlo technique. Recently the data have been re-analyzed¹⁹ to determine F_2 and xF_3 for $0.0075 \leq x \leq 0.75$ and $1.3 \leq Q^2 \leq 126 \text{ GeV}^2$ using the muon and hadron energy calibrations taken directly from test beam data. The updated structure functions corrected for radiative effects, for the non-isoscalarity of the Fe target, for the charm-production threshold and for the mass of the W -boson propagator are shown in Figure 3.

The structure function F_2 from νFe DIS can be compared to F_2 from e and μ DIS for an isoscalar target. To make this comparison, two corrections have been applied to the charged-lepton data. The deuterium data from SLAC, NMC, and BCDMS have been corrected to Fe using the F_2^{lN}/F_2^{lD} ratio from SLAC and NMC. The second correction accounts for the electric charges of the quarks participating in the electromagnetic interactions:

$$\frac{F_2^l}{F_2^\nu} = \frac{5}{18} \left(1 - \frac{3}{5} \frac{s + \bar{s} - c - \bar{c}}{q + \bar{q}} \right) \quad (4)$$

The comparison of F_2 from the charged-lepton and neutrino DIS is shown in Figure 4. The F_2 values generally agree well except in the low x bin (0.0125), where there is a 15% discrepancy between the NMC and CCFR results. It can not be explained by increasing the size of the strange sea, as this is limited by CCFR dimuon data²⁰, however it has been suggested that its distribution may be more complicated than usually assumed. Another possibility is that the nuclear corrections are different for neutrino and charged leptons.

Using the improved F_2 and xF_3 data in the region $Q^2 > 5 \text{ GeV}^2$, $x < 0.7$ and $W^2 > 10 \text{ GeV}^2$, the CCFR collaboration has performed a QCD fit to extract Λ_{QCD} . Target mass corrections were included into the fit. Higher twist (HT) effects were taken into account. The best QCD fit to the data is shown in Figure 3.

From this fit in NLO QCD for 4 quark flavors the value $\Lambda_{\overline{MS}} = 337 \pm 28(\text{exp.}) \pm 13(\text{HT}) \text{ MeV}$ has been obtained, which yields $\alpha_S(M_Z^2) = 0.119 \pm 0.002(\text{exp.}) \pm 0.001(\text{HT}) \pm 0.004(\text{scale})^b$. A fit to the data on xF_3 only, which is not coupled to the gluon distribution, gives $\Lambda_{\overline{MS}} = 381 \pm 53(\text{exp.}) \pm 17(\text{HT}) \text{ MeV}$, which is consistent with the result of the combined fit of F_2 and xF_3 but has larger errors because effectively only half of the data are used. The value of α_S is significantly higher than the earlier CCFR result¹⁸, $\alpha_S(M_Z^2) = 0.111 \pm 0.002(\text{stat.}) \pm 0.003(\text{syst.})$, mainly due to the new energy calibration.

^bThe NNLO analysis²¹ of the new CCFR data on $\nu\text{Fe} \rightarrow lX$ gives a very similar result: $\alpha_S(M_Z^2) = 0.117 \pm 0.002(\text{exp.}) \pm 0.005(\text{syst.}) \pm 0.003(\text{theory})$.

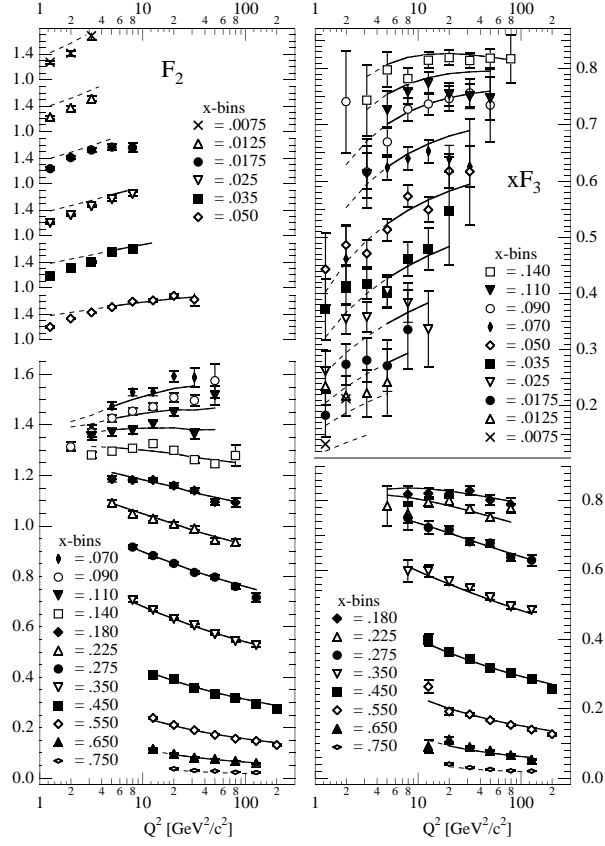


Figure 3: The updated F_2 and xF_3 data from CCFR. The results of a NLO QCD fit are given by the solid line. The dashed line extrapolates the fit to the lower Q^2 region excluded from the fit.

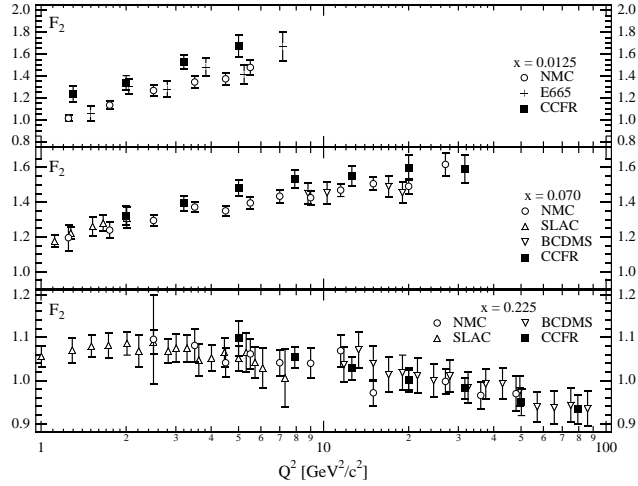


Figure 4: Comparison of the updated CCFR F_2 values for νFe with those for νD from NMC, E665, BCDMS and SLAC. The charged lepton data have been corrected to an isoscalar Fe target and for quark-charge effects.

2.3 Summary for DIS in Fixed Target Experiments

The present fixed target program for unpolarized DIS with charged lepton beams is now completed. The final results of the SLAC, BCDMS, E665, NMC experiments are published providing us with a firm basis for QCD analyses of the nucleon. The neutrino beam data from CCFR at FNAL have been re-analyzed to give new F_2 and xF_3 values. The value of α_s ($\alpha_s \sim 0.119$) extracted from the updated structure function results is significantly higher than the earlier CCFR result ($\alpha_s \sim 0.111$). It is also larger than the result²² based on the SLAC/BCDMS data ($\alpha_s \sim 0.113$) and is very close to the LEP values ($\alpha_s \sim 0.120$). The existing very precise data sets are well consistent apart from a discrepancy of about 15% at low x between the F_2 values derived from the CCFR and the NMC data.

3 Constraints on Parton Densities from Hadron-Hadron Collisions

Information on the valence quark density ratio $u(x)/d(x)$ at high Q^2 and on the $\bar{u}(x)/\bar{d}(x)$ ratio of sea quarks can be gained from W production in $p\bar{p}$ collisions and μ -pair production via the Drell-Yan mechanism in pp and $p\bar{d}$ interactions. Prompt photon and jet data from hadronic collisions are sensitive to the gluon density at large x . Recent preliminary results on these processes from CDF, E866 and E706 are presented in this section.

3.1 Charge Asymmetry in W Production in $p\bar{p}$ Collisions

In $p\bar{p}$ collisions, $W^+(W^-)$ bosons are produced primarily by the annihilation of $u(d)$ quarks in the proton and $\bar{d}(\bar{u})$ quarks from the antiproton. As u quarks carry on average more momentum than d quarks, the W^+ 's tend to follow the direction of the incoming proton and the W^- 's that of the antiproton. The charge asymmetry in the production of W 's as a function of rapidity is related to the u and d quark distributions at $Q^2 \approx M_W^2$. It is roughly proportional to the ratio of the difference and the sum of the quantities $d(x_1)/u(x_1)$ and $d(x_2)/u(x_2)$, where x_1 and x_2 are the fractions of the nucleon momentum carried by the quarks in the p and \bar{p} , respectively. Since the W rapidity is experimentally undetermined, because of the unknown longitudinal momentum of the

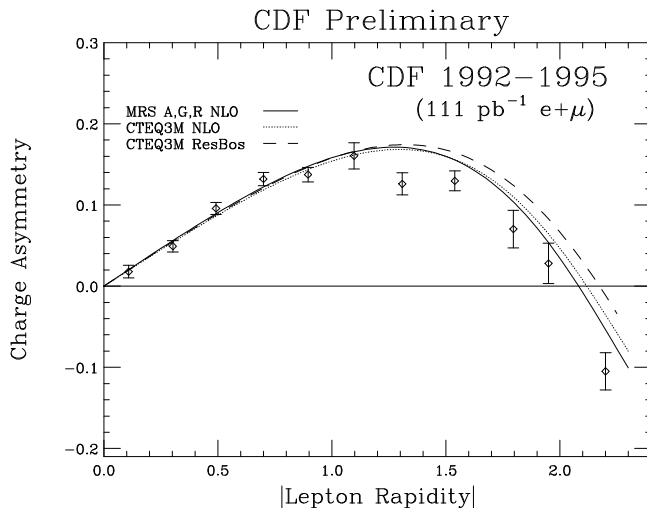


Figure 5: The charge asymmetry $A(y_l)$ corrected for detector effects and backgrounds as a function of the lepton rapidity y_l . Due to CP invariance $A(y_l) = -A(-y_l)$ and the two values are combined. The statistical and systematic errors are added in quadrature.

neutrino from the W decay, the lepton charge asymmetry is actually measured:

$$A(y_l) = \frac{d\sigma^+/dy_l - d\sigma^-/dy_l}{d\sigma^+/dy_l + d\sigma^-/dy_l}, \quad (5)$$

where $d\sigma^+$ ($d\sigma^-$) is the cross section for W^+ (W^-) decay leptons as function of the lepton rapidity y_l .

Previously published W asymmetry results obtained by the CDF collaboration at FNAL²³ have been used already in global analyses^{4,8,11} to extract parameterizations of parton distribution functions in the nucleon. The new preliminary CDF results²⁴ are shown in Figure 5 and are based on the data from 1992 to 1995, corresponding to a five fold increase in statistics. Furthermore the asymmetry measurement is extended to larger rapidity (up to $|y_l| = 2.2$) and provides information on parton densities in a larger x range ($0.006 < x < 0.34$) than previously. As shown in Figure 5, the existing parameterizations are in good agreement with the new measurements in the central region ($|y_l| < 1.1$). However, at large rapidity expectations from global parton distribution analyses are generally above the data.

3.2 Drell-Yan μ -pair Production

Dimuon production via the Drell-Yan mechanism can be used to investigate the question of flavor asymmetry in the nucleon sea. The proton-nucleon Drell-Yan cross section can be written in terms of parton distribution functions as

$$\sigma^{pN} \sim \sum_i e_i^2 [q_i(x_1)\bar{q}_i(x_2) + q_i(x_2)\bar{q}_i(x_1)], \quad (6)$$

where x_1 and x_2 are the fractions of the nucleon momentum carried by the beam and target partons respectively. In the approximation $x_1 \gg x_2$, the ratio of the Drell-Yan yields from protons incident on deuterium and hydrogen targets, $\sigma^{pd}/2\sigma^{pp}$, has a simple approximate relation to \bar{u}/\bar{d} :

$$\frac{\sigma^{pd}}{2\sigma^{pp}} \Big|_{x_1 \gg x_2} \approx \frac{1}{2} \left(1 + \frac{\bar{d}(x_2)}{\bar{u}(x_2)} \right) \quad (7)$$

Preliminary results on the ratio of the deuterium to hydrogen Drell-Yan cross sections from the

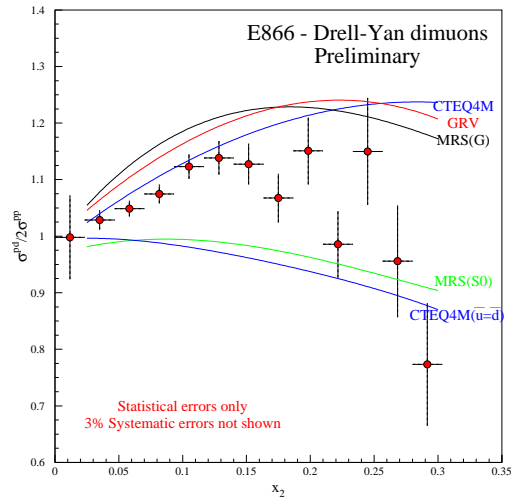


Figure 6: The ratio of the Drell-Yan cross sections on deuterium and hydrogen targets.

FNAL E866 experiment²⁵ are shown in Figure 6 as a function of x_2 . The data points are compared with different parameterizations of the proton. Also plotted is a curve based on CTEQ4M⁹, where the parameterization was modified to force a flavor symmetric sea $\bar{u}_p = \bar{d}_p \equiv (\bar{u}_p + \bar{d}_p)/2$. The preliminary E866 results confirm the results of NMC^{17,13} and NA51²⁶ that $\bar{d}_p > \bar{u}_p$. The data in Figure 6 are compatible with present parameterizations at low x , but for $x > 0.2$ the parameterizations fail. It is the final goal of the E866 experiment to measure the ratio of Drell-Yan cross sections $\sigma^{pd}/2\sigma^{pp}$ with an accuracy of about 1% for $0.05 \leq x \leq 0.15$ and to determine \bar{u}/\bar{d} over the full range up to $x \simeq 0.3$.

3.3 Prompt Photon Production

The prompt photon production $pN \rightarrow \gamma X$ is dominated by the subprocess $qg \rightarrow q\gamma$ and, in leading order, directly related to the gluon density. Recently the E706 experiment at Fermilab presented high statistic measurements²⁷ on large transverse momentum prompt photon and inclusive π^0 cross sections using 530 and 800 GeV proton beams and a 515 GeV π^- beam incident on a Be target. Current NLO QCD calculations failed to describe the data, indicating the presence of a substantial initial state parton transverse momentum (k_T) in the hard scattering (a discussion on the k_T problem can be found in ref.²⁸). A simple implementation of a parton k_T in QCD calculations, using empirical $\langle k_T \rangle$ values consistent with observations, provides a reasonable description of the data. The gluon distribution obtained in the combined fit (taking into account k_T effects) to the DIS, Drell-Yan and E706 prompt photon data is similar to the CTEQ4 result⁹ and consistent with the jet cross section results from CDF and D0. An improved theoretical understanding of soft gluon effects will facilitate the determination of the gluon distribution function at high x .

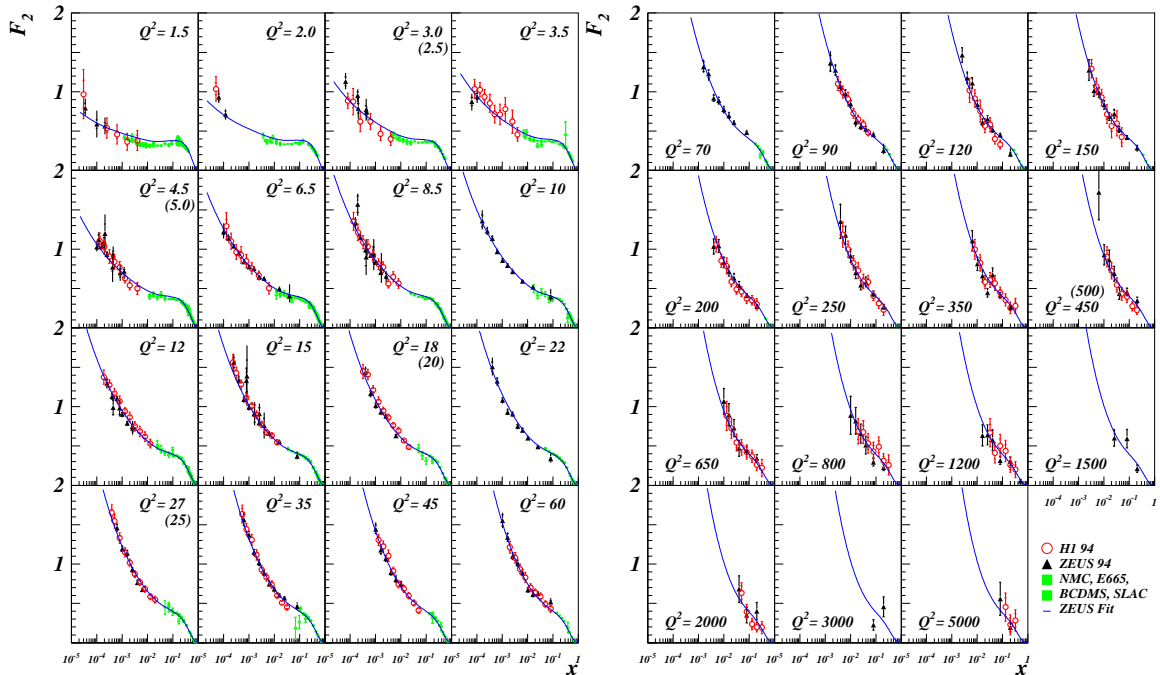


Figure 7: F_2 data from HERA (1994) and fixed target experiments at fixed Q^2 (in GeV^2) as a function of x . The lines correspond to the NLO QCD fit by ZEUS.

4 The HERA Results

Experiments at HERA extended the previously accessible kinematic range up to very large values of $Q^2 > 10^3 \text{ GeV}^2$, and down to very small values of $x < 10^{-4}$ (Figure 1). The first F_2 measurements reported at HERA ^{29,30}, based on data collected in 1992, revealed a pronounced rise of F_2 at low $x < 10^{-2}$ with decreasing x . The rise was confirmed by the much improved data of 1993 ^{31,32}. This rise can be understood as an increase in the quark-antiquark sea which in turn is being driven (eqs. 2, 3) by a rapid increase in the gluon density. Thus, the quantitative investigation of gluon dynamics at low x is one of the major challenges at HERA.

The first substantial data samples, with an integrated luminosity of about 3 pb^{-1} , have been collected in 1994. Using this data, the two HERA experiments, H1 and ZEUS, have published F_2 results ^{33,34,35} covering a range in Q^2 , x , and y , corresponding to $1.5 < Q^2 < 5000 \text{ GeV}^2$, $3 \cdot 10^{-5} < x < 0.5$ and roughly $0.01 < y < 0.6$. In 1995, both ZEUS and H1 have improved their detectors to be able to measure electron scattering angles close to zero. ZEUS added a special detector (BPC) near the beam pipe in the electron beam (backward) direction which allowed to measure F_2 down to $Q^2=0.11 \text{ GeV}^2$ ³⁶. The H1 collaboration replaced the previous electromagnetic

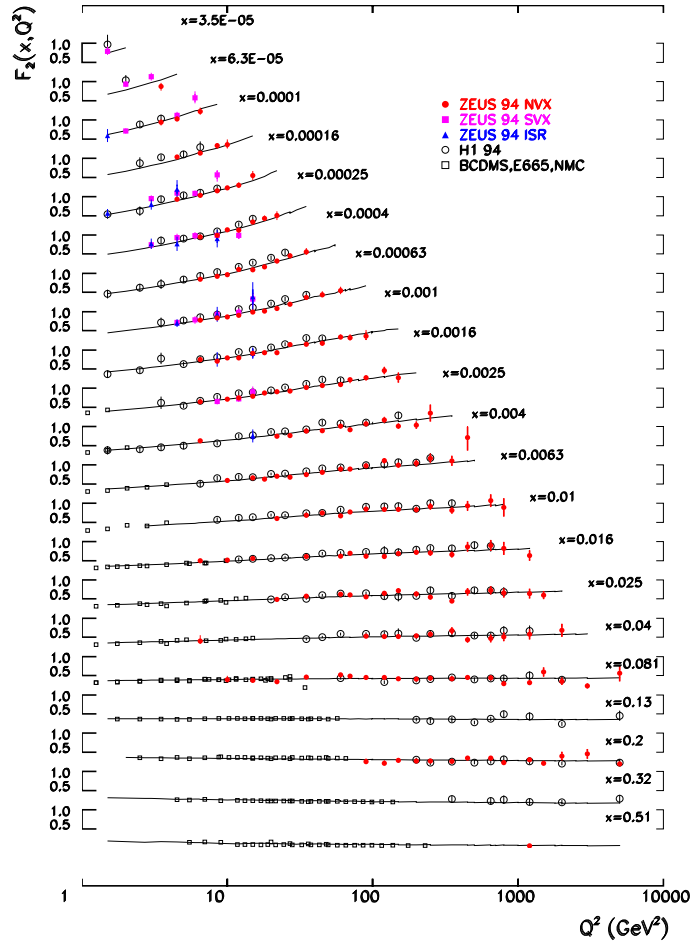


Figure 8: F_2 data from HERA (1994) and fixed target experiments at fixed x as a function of Q^2 . The lines correspond to the NLO QCD fit by ZEUS.

calorimeter in the backward direction by a lead/scintillating fiber calorimeter (SPACAL)³⁷ and measured F_2 down to $Q^2=0.35$ GeV²³⁸ using data collected during a short period in 1995 when the ep collision vertex was shifted by 70 cm in the proton-beam direction with respect to the nominal position. With this new calorimeter, using 1996 data, H1 measured the cross section up to $y=0.82$, where the sensitivity to the longitudinal proton structure function F_L is enlarged (eq. 1). The region of very large $Q^2 > 15000$ GeV², although limited by event statistics, became recently of high interest and is discussed elsewhere^{39,40}.

All existing F_2 data from HERA were analyzed in the framework of perturbative QCD with the goal to determine the gluon distribution. A quantity directly related to the gluon density is the charm contribution $F_2^{c\bar{c}}$ to the structure function of the proton at low x . It was measured by both collaborations. Another quantity related in QCD to the gluon⁴¹ is the longitudinal proton structure function F_L . The H1 collaboration made an attempt to derive F_L from the measured cross section at high y assuming that F_2 is given by a QCD fit to data at lower y . The transition between the region of perturbative QCD (DIS) and Regge phenomenology (photoproduction, $Q^2 = 0$) was studied using the HERA measurements in the very low Q^2 region.

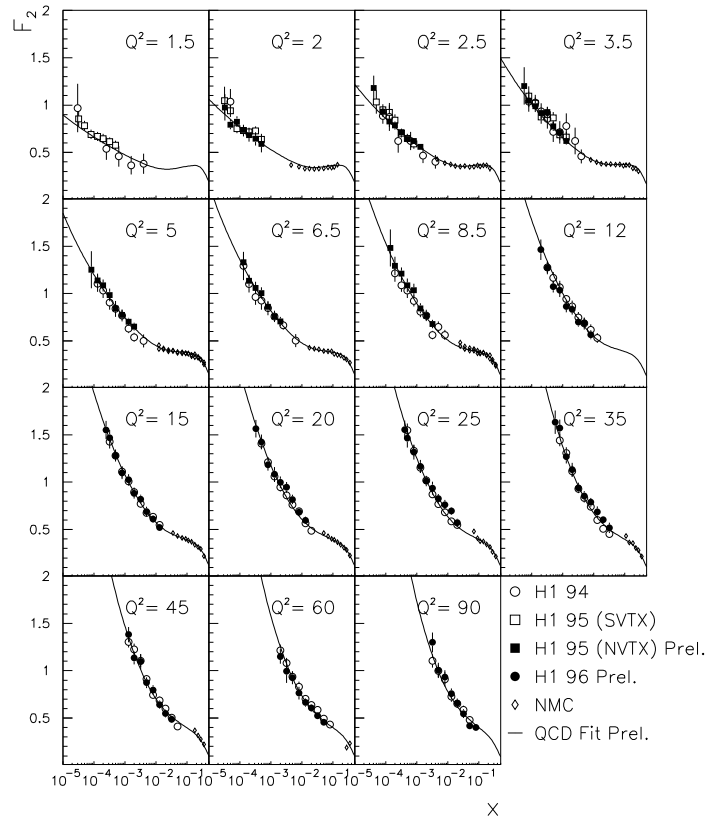


Figure 9: Measurements of F_2 by the H1 experiment. The new data (1995 data for $2 < Q^2 < 8.5$ GeV² and 1996 data for $12 < Q^2 < 90$ GeV²) are in good agreement with the previous results on F_2 . The curves represent the preliminary result of a NLO QCD fit to the H1, NMC and BCDMS structure function data, described in Section 4.2.

4.1 The Proton Structure Function $F_2(x, Q^2)$ at HERA

The HERA results for the structure function F_2 from the 1994 data are shown in Figure 7 as function of x and in Figure 8 as function of Q^2 . F_2 was derived from the ep cross section according to eq. 1. The values of R needed for that were calculated using the QCD relation⁴¹ and the result of a NLO QCD fit (ZEUS) or the GRV parameterization¹¹ (H1). The typical systematic error is around 5% and dominates the total error everywhere apart from the high Q^2 region. The data from H1 and ZEUS are consistent with each other and smoothly connected to data from the fixed target experiments. The step rise of F_2 with decreasing x and the scaling violation are clearly visible in Figure 7 and in Figure 8 respectively. The curves in Figures 7, 8 represent results of the NLO QCD fit by ZEUS.

Figure 9 shows new, preliminary H1 results⁴² on F_2 from the data taken in 1995 and 1996 with ep interactions at the standard (nominal vertex) point. The previous measurements of H1 (from 1994 and shifted vertex running in 1995) and the higher x data of NMC are given as well. There is remarkable agreement with the 1994 data although those were taken with a different apparatus in the backward direction. The curves in Figure 9 represent a NLO QCD fit by H1 which is used for a determination of the gluon density as described below.

The rise of F_2 towards low x has been quantified by determining the exponent λ of $F_2 \propto x^{-\lambda}$ at fixed Q^2 (or equivalently $F_2 \propto W^{2\lambda}$, where $W \approx \sqrt{Q^2/x}$ is the center of mass of the γ^*p system). Figure 10 represents a preliminary update of the previous H1 result^{33,38} on the exponent λ . There is a smooth transition visible from large values of $\lambda \simeq 0.40$ for $Q^2 = 1000 \text{ GeV}^2$ down to $\lambda \simeq 0.15$ for $Q^2 = 1 \text{ GeV}^2$ approaching $\lambda \simeq 0.08$ which has been measured for hadronic and real photoproduction ($Q^2 = 0$) total cross sections. The results from HERA for the transition region between DIS and photoproduction are discussed in detail in section 4.5.

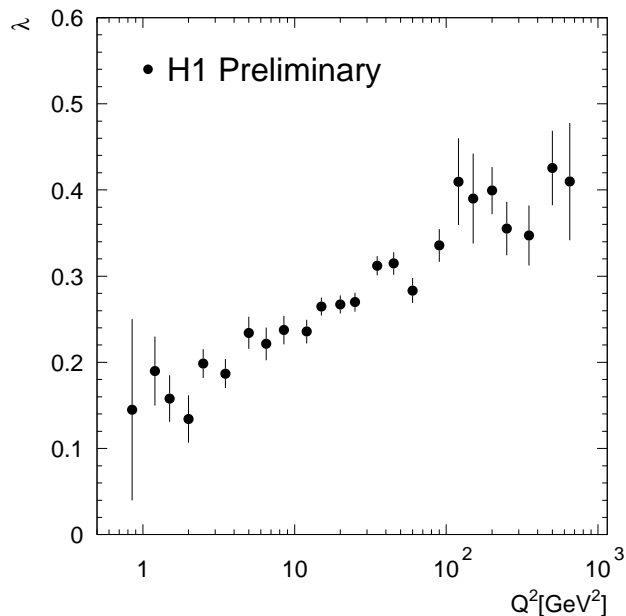


Figure 10: Variation of the exponent λ from fits to the H1 data (1994, 1995 and 1996) of the form $F_2 \propto x^{-\lambda}$ at fixed Q^2 values and $x < 0.1$.

4.2 The Gluon Distribution $xg(x, Q^2)$ at Low x

The scaling violation, which is clearly visible in Figure 8 for the structure function F_2 in the HERA domain at low x , is caused by gluon bremsstrahlung from quarks and quark pair production from gluons and is related to the gluon density. Both the H1 and the ZEUS collaborations performed NLO QCD fits to their F_2 data with the goal to determine the gluon distribution at low x . The fits use the \overline{MS} renormalization scheme with the DGLAP evolution equations³ for three light flavors adding the charm contribution determined in the NLO calculation of the boson gluon fusion (BGF) process⁴³.

The ZEUS fit was performed to ZEUS data³⁴ in the range $1.5 \leq Q^2 \leq 5000 \text{ GeV}^2$. The input scale Q_0^2 was chosen to be 7 GeV^2 , at which the gluon distribution xg , the singlet quark distribution $x\Sigma$ and the difference of up and down quarks in the proton $x\Delta_{ud}$ were parameterized as

$$\begin{aligned} xg(x) &= A_g x^{\delta_g} (1-x)^{\eta_g} (1 + \gamma_g x), \\ x\Sigma(x) &= A_s x^{\delta_s} (1-x)^{\eta_s} (1 + \varepsilon_s \sqrt{x} + \gamma_s x), \\ x\Delta_{ud}(x) &= A_{ns} x^{\delta_{ns}} (1-x)^{\eta_{ns}}. \end{aligned} \quad (8)$$

The strange quark distribution was assumed to be 20% of the sea at $Q^2 = 4 \text{ GeV}^2$ ⁴⁴. The sea quark density is obtained by subtracting the valence distribution (taken from the MRSD- parameterization⁴) from the singlet distribution.

In the present update of the published H1 fit results³³ the starting point of the evolution was chosen to be $Q_0^2 = 1 \text{ GeV}^2$ and all H1 data with $1.5 \leq Q^2 \leq 5000 \text{ GeV}^2$ including the measurements presented at this conference (see previous section) were included in the fit. In order to reduce the influence of the longitudinal structure function a cut of $y < 0.6$ was used for all H1 data sets. The input parton distributions at the starting scale Q_0^2 were parameterized as follows:

$$\begin{aligned} xg(x) &= A_g x^{B_g} (1-x)^{C_g}, \\ xu_v(x) &= A_u x^{B_u} (1-x)^{C_u} (1 + D_u x + E_u \sqrt{x}), \\ xd_v(x) &= A_d x^{B_d} (1-x)^{C_d} (1 + D_d x + E_d \sqrt{x}), \\ xS(x) &= A_S x^{B_S} (1-x)^{C_S} (1 + D_S x + E_S \sqrt{x}), \end{aligned} \quad (9)$$

where $S = \bar{u} + \bar{d}$ and $\bar{u} = \bar{d} = 2\bar{s}$ define the sea distributions.

In order to constrain the valence quark densities at higher x , proton and deuterium data of the muon scattering experiments NMC¹² (H1 and ZEUS fits) and BCDMS⁴⁵ (H1 fit only) were also used. To avoid a possible influence of higher twist effects, data in the range $x > 0.5$ for $Q^2 < 15 \text{ GeV}^2$ were excluded from the H1 fit. The normalizations of all data sets were allowed to vary taking into account the quoted errors.

The resulting gluon distributions as determined by the HERA experiments^{46,42} are shown in Figure 11 for $Q^2 = 20 \text{ GeV}^2$. The error bands account for statistical and systematical errors including correlations. They take also into account possible variations of α_s by ± 0.005 around $\alpha_s = 0.113$ ²² (0.118) in case of ZEUS (H1) and of the charm mass $1.3 < m_c < 1.5 \text{ GeV}$ for ZEUS and $m_c = 1.5 \pm 0.3$ for H1. The agreement between the fit results is good. At the lowest x values, $x \sim 10^{-4}$, the gluon distribution is now determined with a precision of about 10%. At $x \approx 0.01$ the HERA fits make contact with the fit performed by the NMC collaboration on their own data⁴⁷.

The gluon distribution in Figure 11 is rising steeply towards low x . For comparison the gluon densities from the recent parton distributions MRSR1⁶, CTEQ4M⁹ and from GRV94-HO¹¹ are shown in the Figure as well. Whereas the agreement with MRS and CTEQ at low x is good, the gluon obtained from the dynamical evolution by GRV is too steep.

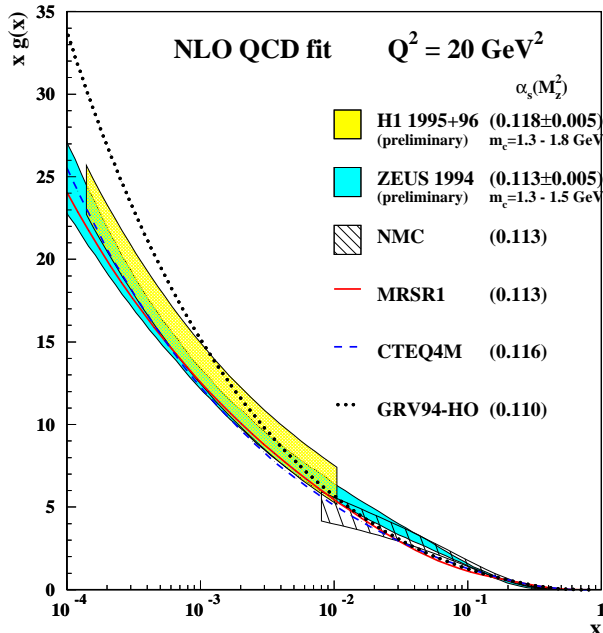


Figure 11: Gluon distributions from the HERA NLO QCD fits to structure function data. The error bands include the statistical and systematic errors and also the uncertainties due to α_s , due to the charm quark mass m_c and due to the loosely constrained behaviour of xg at high $x > 0.1$ (only H1 fit). The NMC fit is also shown at higher x . The MRSR1, CTEQ4M, and GRV94-HO parameterizations are shown for comparison.

In global analyses, non-DIS measurements like prompt photon and/or jet data are generally used to constrain the very high x region (see section 3.3). These data sets have not been included in the HERA fits. This was taken into account by the H1 collaboration as an additional uncertainty which was estimated by a control fit with a five parameter gluon distribution forced to reproduce the high x gluon density of ref.⁵. This leads to a gluon distribution which is lower by nearly 10% at $x = 0.01$ but in very good agreement with the standard three parameter gluon at lower x . The difference of these two determinations has been included in the error band in Figure 11 and is a dominant contribution to the error of xg at x near to 0.01.

4.3 Charm Contribution $F_2^{c\bar{c}}(x, Q^2)$ to the Proton Structure Function

The H1 and ZEUS experiments have published results on open charm production in deep inelastic scattering^{48,49} based on the 1994 data. Recently the ZEUS collaboration presented an update⁵⁰ of their results using the 1995 data, doubling the statistics and widening the Q^2 coverage.

Tagging of charm events is performed by reconstructing D^{*+c} and D^{0d} mesons via their decays into $D^{*+} \rightarrow D^0 \pi_s^+ \rightarrow (K^- \pi^+) \pi_s^+$ and $D^0 \rightarrow K^- \pi^+$, respectively. For the D^{*+} analysis the mass difference $\Delta m = m(D^{*+}) - m(D^0)$, being very close to the π mass, leads to a good resolution and signal to background ratio. A satisfactory suppression of the combinatorial background is obtained also in the D^0 analysis by making use of the hard fragmentation of charm quarks.

The charm contribution $F_2^{c\bar{c}}(x, Q^2)$ to the structure function is obtained by applying the relation

^cCharge conjugates are always implied.

^dThis channel is used only in the H1 experiment.

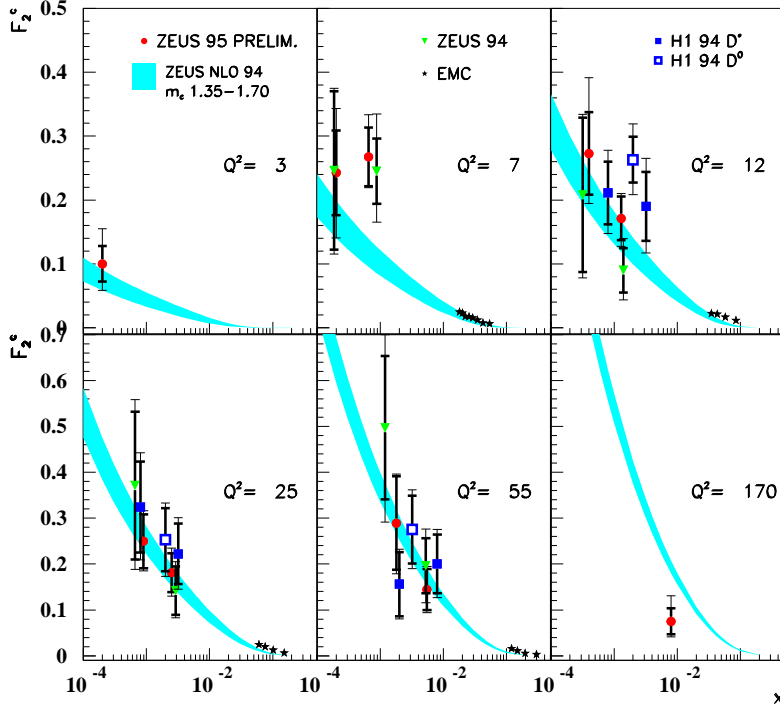


Figure 12: The $F_2^{c\bar{c}}$ results from H1, ZEUS, and EMC are shown as function of x for different bins of Q^2 (in GeV^2). The shaded band represents the NLO calculations with different charm masses based on BGF using the gluon density extracted from the ZEUS NLO DGLAP fit to inclusive F_2 .

to the one photon exchange cross section for charm production

$$\frac{d^2\sigma^{c\bar{c}}}{dx dQ^2} = \frac{2\pi\alpha^2}{Q^4 x} \left(1 + (1-y)^2\right) F_2^{c\bar{c}}(x, Q^2), \quad (10)$$

with the assumption that $R = 0$. $\sigma^{c\bar{c}}$ is obtained from the D^{*+} and D^0 cross sections by integration and extrapolation outside the measured range in transverse momenta and pseudo-rapidities of the D^{*+} , D^0 mesons using NLO calculations⁵¹. The calculations are based on the boson gluon fusion (BGF) production mechanism and the gluon distribution obtained by NLO DGLAP QCD fits to the inclusive F_2 data (see previous section).

Figure 12 shows $F_2^{c\bar{c}}(x, Q^2)$ as measured by H1 and ZEUS together with the EMC results⁵². The HERA measurements extend our knowledge of $F_2^{c\bar{c}}(x, Q^2)$ by two orders of magnitude towards smaller x values. The charm contribution, $F_2^{c\bar{c}}(x, Q^2)$, to the proton structure function is seen to rise by about one order of magnitude from the high x region covered by the fixed target experiment to the low x region measured at HERA. Averaged over the kinematic range at HERA, the ratio $F_2^{c\bar{c}}/F_2$ is about 25%.

In Figure 12 the data are also compared with NLO QCD calculations for $F_2^{c\bar{c}}(x, Q^2)$ shown as a band, where the upper and lower limit corresponds to a charm quark mass of 1.35 and 1.7 GeV, respectively. The measured rise of $F_2^{c\bar{c}}(x, Q^2)$ from the high to the low x region is reasonably described in the three flavor number scheme with charm production via boson gluon fusion. More precise data are needed to study the details of the charm production mechanism and to distinguish between different approaches, MRRS⁷, CTEQ¹⁰ and BMSN⁵³, which provide a consistent treatment of heavy quark production from the threshold region $Q^2 \approx m_q^2$ to the asymptotic region $Q^2 \gg m_q^2$.

The first results from HERA on $F_2^{c\bar{c}}(x, Q^2)$ are very promising. They indicate that the BGF process is dominant. However, high precision results are still to come with high luminosity at HERA and the use of silicon micro-vertex detectors, installed already by H1 and planned by ZEUS for the year 2000, which could improve the detection efficiency by an order of magnitude.

4.4 The Longitudinal Proton Structure Function $F_L(x, Q^2)$

The H1 measurements^{33,35,42} of F_2 , shown in Figure 9 and discussed in section 4.1, were limited to y values below 0.7, and the contribution of F_L to the cross section was estimated by a QCD calculation. At large y the weights of F_2 and F_L in eq. 1 become of comparable size. The H1 collaboration has attempted to reverse that procedure, i.e. to measure the cross section at the maximum possible y and to derive F_L assuming that F_2 can be obtained from a QCD fit to data at lower y .

The measured DIS cross sections for Q^2 between 12 and 35 GeV^2 are shown in Figure 13

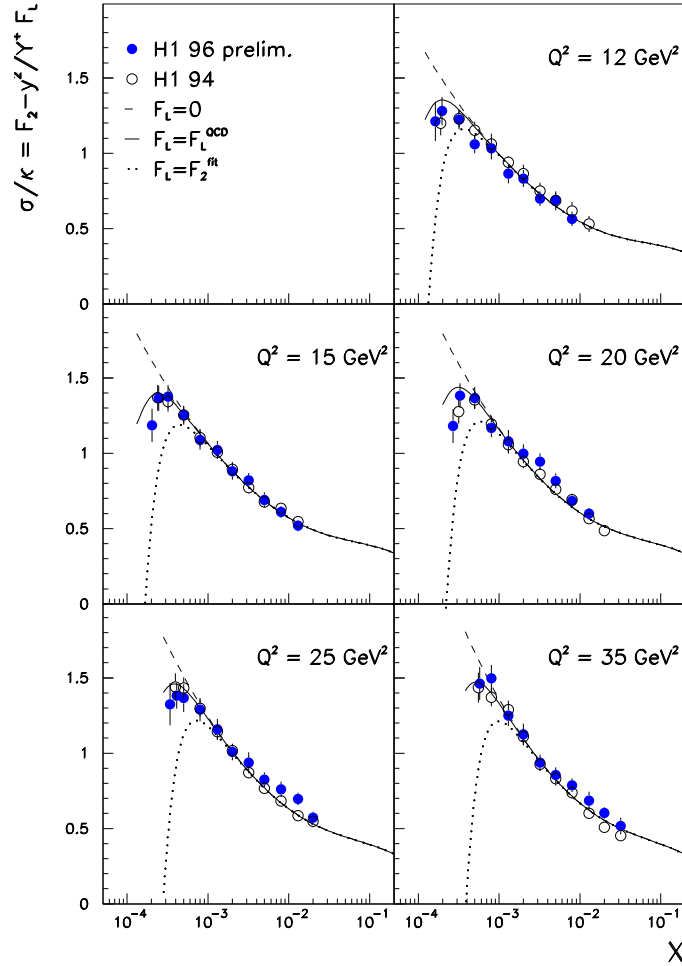


Figure 13: Measurement of the DIS cross section by H1 (1994, 1996) divided by the kinematic factor $\kappa = (2\pi\alpha^2 \cdot Y_+) / (Q^4 x)$, where $Y_+ = 1 + (1 - y)^2$. The solid line shows the QCD calculation of F_2 and of F_L . Also shown are the cross section calculations using the extreme assumptions $F_L = F_2$ (dotted line) and $F_L = 0$ (dashed line). The lowest x points for $12 \leq Q^2 \leq 25 \text{ GeV}^2$ correspond to $y = 0.82$.

comparing the 1994 data (open points) with the preliminary data of 1996 (closed points). The error bars include statistical and systematic errors added in quadrature. Both cross section measurements agree well. The new data extended the y range at four Q^2 values to $y = 0.82$, thus considerably increasing the sensitivity to F_L . The total systematic errors of the cross section at the largest y is 8%, rather independently of Q^2 .

Figure 13 shows also calculations of the cross section using the QCD fit to F_2 , described in section 4.2, and three different assumptions on the longitudinal structure function F_L . The measured cross section is in agreement with the NLO DGLAP calculation apart from large y at $12 \leq Q^2 \leq 25 \text{ GeV}^2$, where the measured points tend to be lower than the QCD expectations (solid lines in Figure 13).

In order to represent the cross section measurement as a determination of F_L , a QCD fit was performed using the new H1 data (1995, 1996) only at low $y < 0.35$ together with the BCDMS and NMC measurements. The F_L values shown in Figure 14 are calculated from the F_2 values determined by this fit and the measured cross sections in the high y region. The F_2 values from this fit agree within 2% with the result of the former fit³⁵ to the H1 (1994) and BCDMS data. For $y = 0.68$ the new result on F_L is in good agreement with the published 1994 data³⁵ (open points).

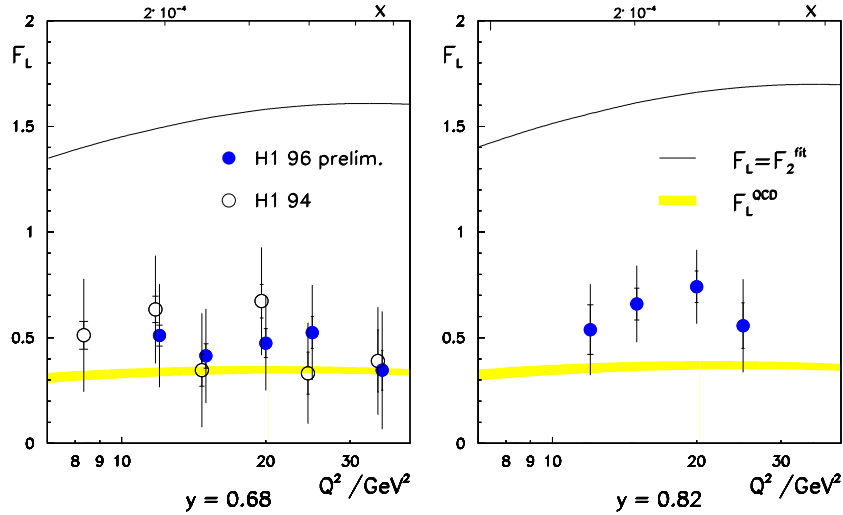


Figure 14: Longitudinal structure function $F_L = (F_2^{QCDfit} - \sigma/\kappa) \cdot Y_+/y^2$, where $\kappa = (2\pi\alpha^2 \cdot Y_+)/ (Q^4 x)$ and $Y_+ = 1 + (1 - y)^2$, determined as function of Q^2 or $x = Q^2/sy$ for $y = 0.68$ and $y = 0.82$. The closed points represent the preliminary H1 (1996) result while the open points are the published H1 (1994) data. The inner error bars are the statistical error. The full error bars include the statistical and systematic errors added in quadrature. The error bands represent the uncertainty of the calculation of F_L using the gluon and quark distributions as determined from a NLO QCD analysis of the new H1 (1995, 1996) data for $y < 0.35$ and the fixed target experiment data. The upper line defines the allowed upper limit of $F_L = F_2$ where F_2 is given by the QCD fit.

The total error of F_L includes three different sources as discussed in ref.³⁵: the uncorrelated part of the systematic error of the high y cross section measurement, the systematic error of the cross section correlated to the error of the input data to the QCD fit and the error due to different assumptions inherent in the QCD fit. Out of the three error contributions the genuine high y cross section uncertainty is the dominating one. The errors of F_L at $y = 0.82$ are smaller than the errors at lower y mainly due to the enhanced sensitivity to F_L (factor y^2 in eq. 1).

The calculation of F_L in NLO QCD is given in Figure 14 by a shaded band. The experimental uncertainty of this calculation is about 6%. The data points are in agreement with QCD expectation,

however, they are systematically higher than expected (note that the points at given y are highly correlated). This tendency is also visible in the cross section measurement at high y (Figure 13).

A determination of F_L at HERA which is free of any theoretical assumptions is foreseen by measuring the ep inclusive cross section at different incident proton beam energies.

4.5 The Very Low Q^2 Region

With improved detectors in the backward region the ZEUS and H1 data on F_2 cover now a range of Q^2 down to ~ 0.1 GeV². These data allow to study the transition from the region of perturbative QCD (DIS) to the photoproduction limit described by Regge phenomenology.

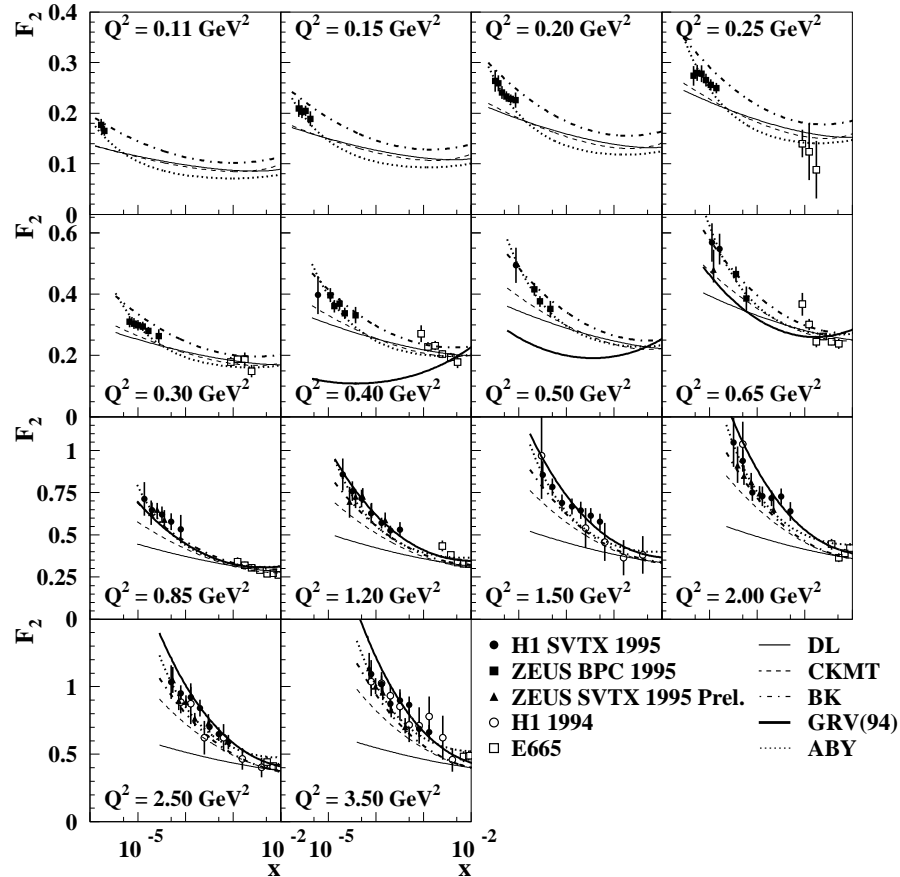


Figure 15: Recent measurements of the proton structure function $F_2(x, Q^2)$ in the low Q^2 region by H1 and ZEUS (full symbols), together with the previous H1 measurements and results from the E665 experiment (open symbols). Different models are compared with the data.

The low Q^2 F_2 results of the HERA experiments are shown in Figure 15. The ZEUS BPC data³⁶ collected in 1995 cover $0.11 < Q^2 < 0.65$ GeV² and $2 \cdot 10^{-6} < x < 6 \cdot 10^{-5}$. The total systematic error varies from 6% to 11% with an overall normalization uncertainty of 2.4%. Here, R is assumed to be 0. The H1 measurements³⁸ based on the shifted vertex running in 1995 cover $0.35 < Q^2 < 3.5$ GeV² and $x > 6 \cdot 10^{-6}$. The total systematic and overall normalization errors are 5-10% and 3%, respectively. The preliminary ZEUS shifted vertex data⁵⁴ from the same period in 1995 cover the region $Q^2 > 0.65$ GeV². In the last two measurements R is taken from ref.⁵⁵. In the

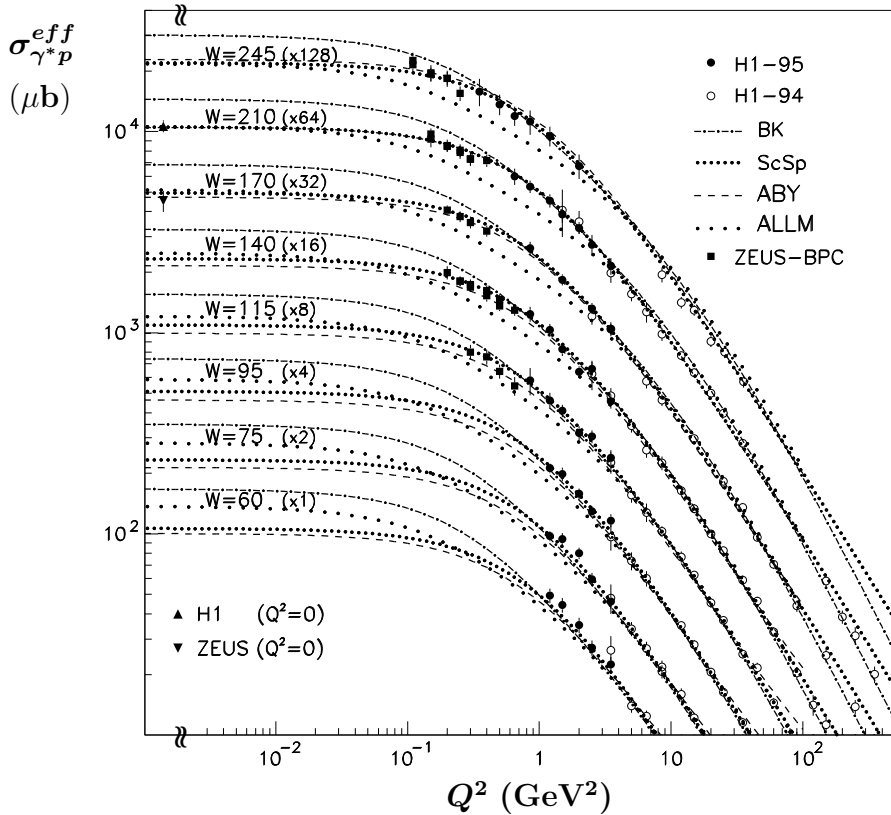


Figure 16: Measurement of the virtual photon-proton cross section $\sigma_{\gamma^*p}^{eff}$ by the HERA experiments as a function of Q^2 at various values of W (in GeV). The photoproduction points as measured at HERA are also given. The cross sections for consecutive W values are multiplied with the factors indicated in the figure (numbers in brackets). The curves represent different predictions for the transition region from DIS to the photoproduction limit ($Q^2=0$).

region of overlap the results are in good agreement. The data also show a smooth continuation from the fixed target measurements towards the low x region at HERA. The rise of F_2 with decreasing x is very strong for values of $Q^2 \geq 2 \text{ GeV}^2$ but becomes less steep for smaller Q^2 values.

Several parameterizations based on phenomenological models are also shown in Figure 15. Most of them use ingredients both from Regge theory at low Q^2 and from QCD when Q^2 is of the order of 1 GeV^2 or larger (for a recent review, see e.g. ⁵⁶).

Parameterizations motivated by Regge theory relate the structure function to Reggeon exchange phenomena which successfully describe the slow rise of the total cross section with energy in hadron-hadron and γp interactions. Using the “bare” instead of the “effective” pomeron intercept, the CKMT ⁵⁷ parameterization rises faster with x compared to the DL ⁵⁸ calculations. Regge inspired models generally undershoot the data, except for the smallest Q^2 values where the calculations approach the data.

Also shown in Figure 15 are the predictions from the QCD-based GRV model ¹¹. This model assumes that all parton distributions at a very low $Q_0^2 = 0.34 \text{ GeV}^2$ have a valence like shape, i.e. vanish for $x \rightarrow 0$, and that the leading twist QCD evolution equations can be used to evolve the parton distributions from this low Q_0^2 scale to larger Q^2 values. Figure 15 shows that the GRV distributions describe the data for $Q^2 \geq 1 \text{ GeV}^2$, but systematically undershoot the data for

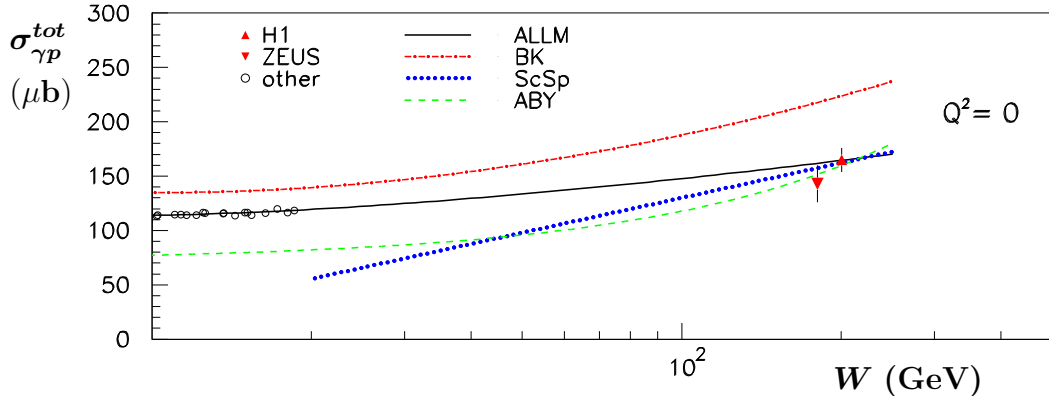


Figure 17: Measurement of the real photon-proton total cross section $\sigma_{\gamma p}^{tot}$ as a function of W .

$Q^2 < 1 \text{ GeV}^2$.

In studies of the whole transition region starting from $Q^2=0$ it is convenient to present the low Q^2 data in terms of a virtual photon-proton cross section⁵⁹. The double differential ep cross section, eq. 1, can be expressed via the absorption cross sections for transverse and longitudinal virtual photons,

$$\frac{d^2\sigma}{dx dQ^2} = \Gamma[\sigma_T(x, Q^2) + \epsilon(y)\sigma_L(x, Q^2)] \equiv \Gamma\sigma_{\gamma^*p}^{eff}(x, y, Q^2). \quad (11)$$

At small x the following relations hold for the flux factor Γ and the photon polarization ϵ : $\Gamma = \alpha(2 - 2y + y^2)/(2\pi Q^2 x)$, $\epsilon(y) = 2(1 - y)/(2 - 2y + y^2)$. The quantity $\sigma_{\gamma^*p}^{eff}$ is the effective measured virtual photon-proton cross section for ep collisions in the defined kinematic range, and can be determined from the data without assumptions on R . The total virtual photon-proton cross section, which is related to F_2 by $\sigma_{\gamma^*p}^{tot} = \sigma_T + \sigma_L \simeq (4\pi^2\alpha/Q^2)F_2(x, Q^2)$, depends only on Q^2 and x (or $W^2 = Q^2(1/x - 1)$). With the exception of the region of high y , where effects of R are sizable, $\sigma_{\gamma^*p}^{tot} \approx \sigma_{\gamma^*p}^{eff}$.

Figure 16 shows the measured $\sigma_{\gamma^*p}^{eff}$ as a function of Q^2 for W values above 60 GeV including the photoproduction results^{60,61} from HERA. The parameterization of Abramowicz et al. (ALLM⁶²) agrees well with the photoproduction data and the measurements at $Q^2 > 2 \text{ GeV}^2$, but departs from the data around $Q^2 = 1 \text{ GeV}^2$.

Also shown in Figure 16 are the predictions of the following models. The model of Badelek and Kwiecinski (BK⁶³) combines the concepts of Generalized Vector Meson Dominance (GVMD) with dynamical parton models such as that of GRV. A GVMD inspired approach has been proposed by Schildknecht and Spiesberger (ScSp⁶⁴) to fit the low and medium Q^2 HERA data up to Q^2 values of 350 GeV^2 . A different approach to the low Q^2 behaviour in the transition region has been presented by Adel et al. (ABY⁶⁵). It assumes that perturbative QCD evolution is applicable to the lowest values of Q^2 . All these models describe the HERA data rather well for Q^2 above $\approx 0.1 - 0.4 \text{ GeV}^2$ but they fail to describe the photoproduction $\sigma_{\gamma p}^{tot}$ data at low $W < 20 \text{ GeV}$ as it is shown in Figure 17. Thus, it turns out that there is no model found which is able to describe all existing data in a consistent way. However, there is a remarkable theoretical activity (e.g. refs.^{66,67,68}) in this field and progress can be expected soon.

5 Summary and Concluding Remarks

With the final results by the NMC experiment on $\mu N \rightarrow \mu X$ deep inelastic scattering, the present fixed target program for unpolarized DIS with charged lepton beams is completed, providing very precise data sets which cover $0.2 < Q^2 < 260 \text{ GeV}^2$ and $8 \cdot 10^{-4} < x < 0.9$. The CCFR collaboration re-analyzed their $\nu Fe \rightarrow \mu X$ data and presented new results on F_2 and xF_3 . The data sets from the different fixed target experiments and from HERA (though the region of overlap is small) are well consistent apart from a difference of about 15% in F_2 between NMC and CCFR at $x=0.0125$. The updated $\alpha_S(M_Z^2)$ value $0.119 \pm 0.002(\text{exp.}) \pm 0.004(\text{theory})$ from the re-analyzed CCFR data on F_2 and xF_3 is close to the LEP results.

The Fermilab experiments CDF, E866 and E706 presented new preliminary results on the charge asymmetry in W production, Drell-Yan μ -pair production and prompt photon production, which provide more stringent constraints on u/d and \bar{u}/\bar{d} ratios and the gluon density at high x .

The H1 and ZEUS experiments at HERA extended the previously accessible kinematic range for F_2 up to very large values of Q^2 and down to very small values of x covering the region $0.1 < Q^2 < 5000 \text{ GeV}^2$ and $2 \cdot 10^{-6} < x < 0.5$. The conventional NLO DGLAP evolution describes the DIS data very well down to surprisingly low Q^2 values of about 1 GeV^2 . Although there is no evidence for deviations from NLO DGLAP, other approaches like the BFKL⁶⁹ or CCFM⁷⁰ evolutions (the latter combines both DGLAP and BFKL) can not be ruled out. Another possible complication at low x is due to higher twist terms which may not be negligible even at Q^2 as large as 10 GeV^2 as discussed in refs.^{71,72} and the success of DGLAP fits, perhaps, reflects the flexibility in choosing arbitrary functions of x for the input parton distributions.

The analysis of the HERA data in the framework of perturbative QCD using NLO DGLAP evolution led to a determination of the gluon distribution at low x . The gluon density is rising steeply towards low x , as one could expect from the strong rise of F_2 with decreasing x . H1 and ZEUS measured the charm contribution $F_2^{c\bar{c}}$ to the structure function of the proton which is directly related to the gluon density at low x . The charm contribution to F_2 is found to be $\approx 25\%$ and the results are reasonably described in the three flavor number scheme with charm production via boson gluon fusion using the gluon densities determined at HERA. Another quantity related to the gluon density is the longitudinal proton structure function F_L . H1 made an attempt to derive F_L from the measured cross section at high y , assuming that F_2 is given by a NLO QCD fit to the data at lower y . The F_L values are in broad agreement with QCD expectation, however, systematically somewhat higher than expected.

The HERA measurements in the transition region from DIS to the photoproduction limit have been confronted with different models. There is no model found which is able to describe all existing data in a consistent way, but further development of models is in progress.

6 Acknowledgements

It is a pleasure for me to thank all my colleagues from NMC, CCFR, CDF, E866, E706, ZEUS and H1 for providing information. Special thanks to the H1 people working on structure function measurements for their tremendous efforts to meet the date with new results. I wish to thank R. Eichler for encouragement and A. Wagner for support, M. Ryskin for long and fruitful discussions, J. Bartels, Yu. Dokshitzer, R. Engel, E. Levin, A.D. Martin, A. Priniias, A. Quadt, J. Smith, B. Surrow for helpful conversations and J. Gayler and A. Zhokin for help in the preparation of the manuscript. My thanks to A. Caldwell, A. De Roeck, M. Klein and A. Levy for careful reading of the final version of the manuscript.

References

1. W. Panofsky, Proc. of the 14th Conference on HEP, Vienna (1968) 23;
E.D. Bloom *et al.*, *Phys. Rev. Lett.* **23**, 930 (1969).
2. D.J. Fox *et al.*, *Phys. Rev. Lett.* **33**, 1504 (1974);
Y. Watanabe *et al.*, *Phys. Rev. Lett.* **35**, 898 (1975).
3. Yu. L. Dokshitzer, *Sov. Phys. JETP* **46**, 641 (1977);
V.N. Gribov and L.N. Lipatov, *Sov. J. Nucl. Phys.* **15**, 438 and 675 (1972);
G. Altarelli and G. Parisi, *Nucl. Phys. B* **126**, 298 (1977).
4. A. Martin, R. Roberts and W. Stirling, *Phys. Rev. D* **50**, 6734 (1994).
5. A.D. Martin, R.G. Roberts and W.J. Stirling, *Phys. Lett. B* **387**, 419 (1996).
6. A. Martin, R. Roberts and W. Stirling, DTP/96/44, RAL-TR-96-037.
7. A.D. Martin, R.G. Roberts, M.G. Ryskin and W.J. Stirling, hep-ph/9612449.
8. H.L. Lai *et al.*, *Phys. Rev. D* **51**, 4763 (1995).
9. H.L. Lai *et al.*, *Phys. Rev. D* **55**, 1280 (1997).
10. H.L. Lai and W.K. Tung, *Z. Phys. C* **74**, 463 (1997).
11. M. Glück, E. Reya and A. Vogt, *Z. Phys. C* **67**, 433 (1995);
A. Vogt, Proc. of the Workshop on Deep-Inelastic Scattering and QCD, Paris (1995) 261.
12. NMC Collab., M. Arneodo *et al.*, *Nucl. Phys. B* **483**, 3 (1997).
13. NMC Collab., M. Arneodo *et al.*, *Nucl. Phys. B* **487**, 3 (1997).
14. NMC Collab., M. Arneodo *et al.*, *Nucl. Phys. B* **481**, 3 (1996).
15. NMC Collab., M. Arneodo *et al.*, *Nucl. Phys. B* **481**, 23 (1996).
16. NMC Collab., M. Arneodo *et al.*, *Phys. Lett. B* **364**, 107 (1995).
17. NMC Collab., M. Arneodo *et al.*, *Phys. Rev. D* **50**, R1 (1994).
18. CCFR Collab., P.Z. Quintas *et al.*, *Phys. Rev. Lett.* **71**, 1307 (1993).
19. CCFR Collab., contributed paper to the LP'97 conference, LP125 (1997); hep-ex/9701017;
W.S. Seligman, Ph.D. thesis, Columbia University, Nevis-292 (1997).
20. CCFR Collab., A.O. Bazarko *et al.*, *Z. Phys. C* **65**, 189 (1995).
21. A.L. Kataev *et al.*, contributed paper to the LP'97 conference, LP075 (1997); hep-ph/9706534.
22. M. Virchaux and A. Milsztajn, *Phys. Lett. B* **274**, 221 (1992).
23. CDF Collab., F. Abe *et al.*, *Phys. Rev. Lett.* **74**, 850 (1995).
24. CDF Collab., CDF/PUB/ELECTROWEAK/PUBLIC/3979 (1997).
25. R.A. Towell, to be published in the proceedings of the Workshop on DIS, Chicago, April 1997.
26. NA51 Collab., A. Baldit *et al.*, *Phys. Lett. B* **332**, 244 (1994).
27. E706 Collab., contributed paper to the LP'97 conference, LP055 (1997).
28. J. Huston *et al.*, *Phys. Rev. D* **51**, 6139 (1995).
29. H1 Collab., I. Abt *et al.*, *Nucl. Phys. B* **407**, 515 (1993).
30. ZEUS Collab., M. Derrick *et al.*, *Phys. Lett. B* **316**, 412 (1993).
31. H1 Collab., T. Ahmed *et al.*, *Nucl. Phys. B* **439**, 471 (1995).
32. ZEUS Collab., M. Derrick *et al.*, *Z. Phys. C* **65**, 379 (1995).
33. H1 Collab., S. Aid *et al.*, *Nucl. Phys. B* **470**, 3 (1996).
34. ZEUS Collab., M. Derrick *et al.*, *Z. Phys. C* **72**, 399 (1996), *Z. Phys. C* **69**, 607 (1996).
35. H1 Collab., C. Adloff *et al.*, *Phys. Lett. B* **393**, 452 (1997).
36. ZEUS Collab., J. Breitweg *et al.*, DESY 97-135 (1997).
37. H1 SPACAL-Group, *Nucl. Instrum. Methods A* **374**, 149 (1996).
38. H1 Collab., C. Adloff *et al.*, *Nucl. Phys. B* **497**, 3 (1997).
39. B. Straub, to be published in the proc. of the LP'97 conference, Hamburg, July 1997.
40. E. Elsen, to be published in the proc. of the EPS HEP 97 conference, Jerusalem, August 1997.
41. G. Altarelli and G. Martinelli, *Phys. Lett. B* **76**, 89 (1978).

42. H1 Collab., contributed paper to EPS HEP 97, paper 260, Jerusalem, August 1997.
43. E. Laenen *et al.*, *Nucl. Phys. B* **392**, 162 (1993);
S. Riemersma *et al.*, *Phys. Lett. B* **347**, 143 (1995).
44. CCFR Collab., C. Foudas *et al.*, *Phys. Rev. Lett.* **64**, 1207 (1994);
S.A. Rabinowitz *et al.*, *Phys. Rev. Lett.* **70**, 132 (1993).
45. BCDMS Collab., A.C. Benvenuti *et al.*, *Phys. Lett. B* **223**, 485 (1989); CERN-EP/89-06.
46. M. Botje, to be published in the proceedings of the Workshop on DIS, Chicago, April 1997.
47. NMC Collab., M. Arneodo *et al.*, *Phys. Lett. B* **309**, 222 (1993).
48. H1 Collab., C. Adloff *et al.*, *Z. Phys. C* **72**, 593 (1996).
49. ZEUS Collab., J. Breitweg *et al.*, DESY 97-089 (1997), accepted by *Phys.Lett.*
50. J. Roldán, to be published in the proceedings of the Workshop on DIS, Chicago, April 1997.
51. B.W. Harris and J. Smith, *Nucl. Phys. B* **452**, 109 (1995).
52. EMC Collab., J.J. Aubert *et al.*, *Nucl. Phys. B* **231**, 31 (1983).
53. M. Buza, Y. Matiounine, J. Smith, W.L. van Neerven, DESY 97-124 (1997).
54. B. Surrow, to be published in the proceedings of the Workshop on DIS, Chicago, April 1997.
55. B. Badelek, J. Kwiecinski and A. Stasto, *Z. Phys. C* **74**, 297 (1997).
56. A. Levy, Proc. of the Workshop on DIS, Rome (1996) 144; A. Levy, DESY 97-013 (1997).
57. A. Capella *et al.*, *Phys. Lett. B* **337**, 358 (1994).
58. A. Donnachie and P.V. Landshoff, *Z. Phys. C* **61**, 139 (1994).
59. L.N. Hand, *Phys. Rev.* **129**, 1834 (1963).
60. H1 Collab., T. Aid *et al.*, *Z. Phys. C* **69**, 27 (1995).
61. ZEUS Collab., M. Derrick *et al.*, *Z. Phys. C* **63**, 408 (1994).
62. H. Abramowicz, E.M. Levin, A. Levy and U. Maor, *Phys. Lett. B* **269**, 465 (1991);
A. Marcus, Ph.D. thesis Tel-Aviv University, TAUP 2350-96 (1996) (unpublished).
63. B. Badelek and J. Kwiecinski, *Phys. Lett. B* **295**, 263 (1992).
64. D. Schildknecht and H. Spiesberger, Bielefeld Uni. preprint BI-TP-97-25 (1997).
65. K. Adel, F. Barreiro and F.J. Yndurain, FTUAM preprint 96-39 (1996).
66. E. Gotsman, E.M. Levin and U. Maor, DESY 97-154 (1997).
67. H. Abramowicz and A. Levy, to be published.
68. A. Martin, M. Ryskin and A. Stasto, to be published.
69. V. Fadin, E. Kuraev and L. Lipatov, *Sov. Phys. JETP* **44**, 443 (1976),
V. Fadin, E. Kuraev and L. Lipatov, *Sov. Phys. JETP* **45**, 199 (1977);
Y. Balitski and L. Lipatov, *Sov. J. Nucl. Phys.* **28**, 822 (1978).
70. M. Ciafaloni, *Nucl. Phys. B* **296**, 49 (1988);
G. Marchesini, *Nucl. Phys. B* **445**, 49 (1995);
S. Catani, F. Fiorani and G. Marchesini, *Nucl. Phys. B* **336**, 18 (1990).
71. E. Levin, to be published in the proceedings of the Workshop on DIS, Chicago, April 1997.
72. J. Bartels and C. Bontus, to be published in the proc. of the Workshop on DIS, Chicago, April 1997.